Secondary Structure and Topology of *Acanthamoeba* Profilin I As Determined by Heteronuclear Nuclear Magnetic Resonance Spectroscopy†

Sharon J. Archer,‡ Valda K. Vinson,§ Thomas D. Pollard,§ and Dennis A. Torchia*,‡

Bone Research Branch, National Institute of Dental Research, National Institutes of Health, Bethesda, Maryland 20892, and Department of Cell Biology and Anatomy, The Johns Hopkins University School of Medicine, Baltimore, Maryland 21205

Received March 8, 1993; Revised Manuscript Received May 6, 1993

ABSTRACT: The protein profilin binds to both actin and the head groups of poly(phosphoinositide)s and may regulate both actin assembly and the phosphoinositide signaling pathway. As a first step in understanding the activity of profilin at the molecular level, we have determined the secondary structure of *Acanthamoeba* profilin I in solution using multidimensional, heteronuclear NMR spectroscopy. Using a combination of triple-resonance (^1H, ^{13}C, ^{15}N) experiments, we obtained virtually complete backbone and side-chain resonance assignments based solely on scalar couplings. 3D and 4D NOESY experiments were then used to determine the secondary structure and global fold of *Acanthamoeba* profilin I. The central feature of the protein structure is a five-stranded antiparallel β-sheet flanked by three helices and a short two-stranded antiparallel β-sheet.

The profilins were originally identified for their ability to bind actin monomers and to regulate the polymerization of actin filaments (Carlsson et al., 1977). Recently it has been shown that profilins associate with plasma membranes (Hartwig et al., 1989) and bind to phosphatidylinositol 4,5-bisphosphate (PIP_2)[1] and phosphatidylinositol 4-phosphate (PIP) (Goldschmidt-Clermont et al., 1990; Machesky et al., 1990). It is believed that profilins may be involved in signal transduction across the membrane (Goldschmidt-Clermont et al., 1991). Knowledge of the structure of profilins would help to understand these activities of the profilins in greater detail. As a first step toward this goal, we used high-resolution NMR spectroscopy to determine the resonance assignments and secondary structure of *Acanthamoeba* profilin I in solution.

Powerful new triple-resonance (^1H, ^{13}C, ^{15}N) NMR techniques enable one to assign proteins having M_r in the range 13000–30000 in an efficient manner, provided that the protein is uniformly enriched with ^{13}C and ^{15}N (Pelton et al., 1991; Grzesiek et al., 1992; Bax & Grzesiek, 1993). Proteins expressed in bacterial systems can be uniformly enriched with ^{15}N and ^{13}C by growing the bacterial cells on minimal media with ^{15}N-labeled ammonium chloride and ^{13}C-labeled glucose. Sequential resonance assignments based on the new triple-resonance experiments rely solely on scalar couplings, thus removing ambiguities that are sometimes encountered when using NOEs to sequentially assign protein resonances. These triple-resonance experiments all correlate side-chain ^1H and ^{13}C resonances to backbone amide N/HN resonances, such that all experiments are referenced to the 2D ^1H–^{15}N HSQC experiment, which simplifies data analysis. Once sequential resonance assignments are known, the structure of the protein is determined from interproton distance constraints, dihedral angle constraints, and hydrogen-bonding patterns (Wüthrich, 1986; Clore et al., 1989). Herein, we report the sequential resonance assignments for *Acanthamoeba* profilin I using triple-resonance NMR techniques. In addition, we report the secondary structure and folding topology of *Acanthamoeba* profilin I in solution as determined from NOESY experiments, $^3J_{HNH\alpha}$ coupling constants, and hydrogen exchange data.

MATERIALS AND METHODS

Sample Preparation. Recombinant *Acanthamoeba* profilin I was prepared with *Escherichia coli* (strain BL21) with the T7 expression vector (Kaiser et al., in preparation). Uniform ^{15}N enrichment or $^{15}N/^{13}C$ enrichment was accomplished by growing the bacteria in M9 minimal medium with $^{15}NH_4Cl$ or $^{15}NH_4Cl$ and D-[$^{13}C_6$]glucose (Cambridge Isotopes, Cambridge, MA). The protein was purified as described previously (Kaiser et al., 1989; Kaiser et al., in preparation). A total of ca. 20 mg of purified, active, ^{15}N-enriched or $^{15}N/^{13}C$-enriched profilin was obtained from each 1 L of cell growth.

To prepare the protein for NMR spectroscopy, 30 μL of D_2O was added to ca. 400 μL of 1.4 mM profilin in H_2O. The pH of the protein sample was adjusted to 6.45 using dilute HCl or NaOH. To prepare a protein sample in D_2O, the protein sample was lyophilized to remove water, dissolved in 0.5 mL of 99.996% D_2O, incubated at 37 °C overnight, and lyophilized a second time. The protein was then dissolved in 99.996% D_2O. The protein concentration of the samples was ca. 1.3 mM. Sample volumes were ca. 430 μL in 5-mm Wilmad NMR tubes (Wilmad Glass Company, Buena, NJ) or 230 μL in restricted-volume Shigemi NMR tubes (Shigemi Standard & Joint Co. Ltd., Tokyo). Samples were stored at 4 °C.

NMR Spectroscopy. NMR spectra of profilin were acquired on Bruker AMX 500 and 600 spectrometers. 2D

† This work was supported by the AIDS Targeted Antiviral Program of the Office of the Director of the National Institutes of Health (to D.A.T.), Public Health Service National Research Service Award GM13620 (to S.J.A.), and NIH Research Grant GM-35171 (to E. E. Lattman and T.D.P.).

‡ National Institutes of Health.

§ The Johns Hopkins School of Medicine.

[1] Abbreviations: CBCA(CO)NH, C^β to C^α to carbonyl to amide N/HN correlation experiment; CBCANH, C^β to C^α to amide N/HN correlation experiment; C(CO)NH, side-chain carbon DIPSI transfer to C^α to carbonyl to amide N/HN correlation experiment; H(CCO)NH, side-chain proton to side-chain carbon DIPSI transfer to C^α to carbonyl to amide N/HN correlation experiment; CT, constant time; HMQC, heteronuclear multiple quantum correlation; HOHAHA, homonuclear Hartmann–Hahn; HSQC, heteronuclear single quantum correlation; NMR, nuclear magnetic resonance; NOE, nuclear Overhauser effect; NOESY, NOE spectroscopy; PIP, phosphatidylinositol 4-phosphate; PIP_2, phosphatidylinositol 4,5-bisphosphate; 2D, two-dimensional; 3D, three-dimensional; 4D, four-dimensional.

0006-2960/93/0432-6680$04.00/0

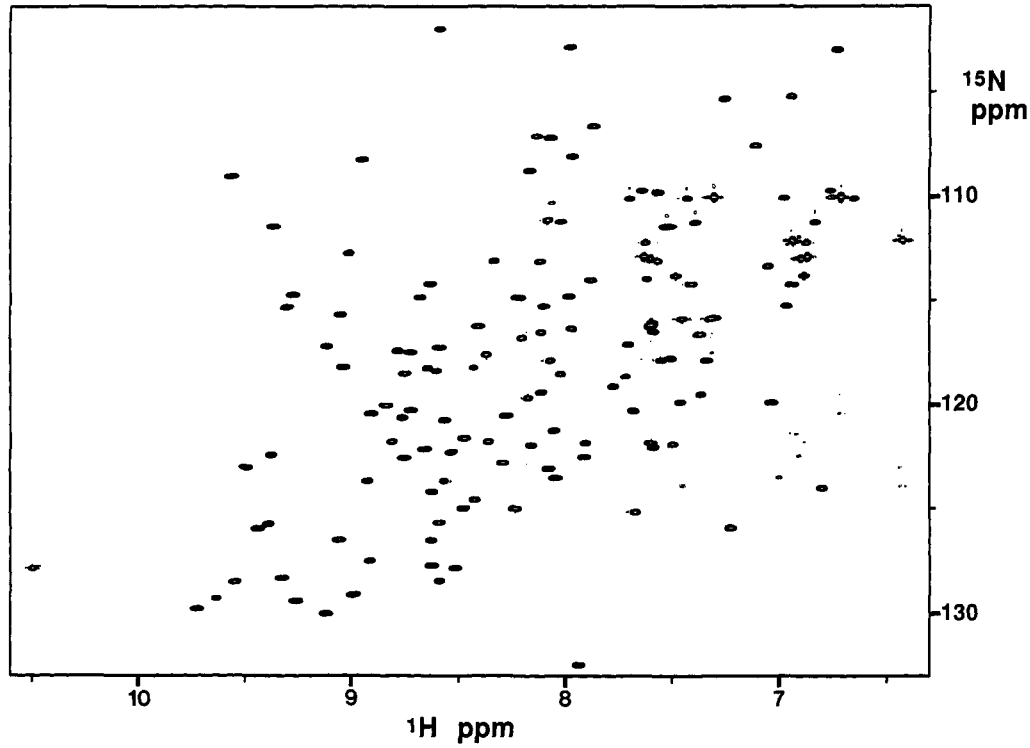

FIGURE 1: ^1H–^{15}N HSQC spectrum of uniformly ^{15}N-enriched profilin. The spectrum was acquired at 500 MHz with 512 complex points in t_2 and 400 complex points in t_1. The spectrum was processed with Lorentzian to Gaussian digital filtering and zero-filled once in each dimension. All peaks in the spectrum were assigned and are listed in Table I.

NMR spectra were processed using Bruker and NMR (New Methods Research, Inc., Syracuse, NY) software available on ASPECT 1000 and SUN data stations, respectively. Multidimensional NMR spectra were processed using a combination of in-house (Kay et al., 1989; S. Grzesiek, unpublished; G. W. Vuister, unpublished) and NMRi software and were analyzed and plotted using in-house software (Garrett et al., 1991).

All spectra were acquired at 30 °C and at 500 MHz unless noted otherwise. 2D HOHAHA (Braunschweiler & Ernst, 1983; Bax & Davis, 1985) spectra were acquired in D_2O with a WALTZ-17 mixing sequence (Bax & Davis, 1985), with mixing times of 17 and 60 ms.

2D ^1H–^{15}N HSQC (Bodenhausen & Ruben, 1980) spectra were acquired on uniformly ^{15}N-labeled profilin in 93% H_2O/7% D_2O at 30 and 37 °C. The water signal was suppressed using presaturation ($\gamma B_2/2\pi$ ca. 20 Hz) and a 1-ms spin-lock pulse (Messerle et al., 1989). 2D ^1H–^{15}N HMQC-J spectra were acquired to determine $^3J_{HNH\alpha}$ coupling constants, as described previously (Kay & Bax, 1990). Amide hydrogen exchange rates were determined by lyophilizing the protein from H_2O, dissolving the protein in D_2O, and acquiring a series of 2D ^1H–^{15}N HSQC spectra at 0.15, 0.5, 1, 2, 4, 8, 16, 25, and 121 h.

2D ^1H–^{13}C CT-HSQC spectra of uniformly $^{13}C/^{15}N$-labeled profilin in D_2O were acquired as described by Vuister and Bax (1992). 2D ^1H–^{13}C CT-HSQC spectra optimized for aromatic resonances were acquired with the inept transfer delay set to 1.6 ms (slightly less than $^1/_4J_{CH(arom)}$) and the constant-time carbon evolution period set to 18.2 ms to refocus the carbon–carbon couplings of 55 Hz. The spectra were acquired with the ^1H carrier set at 7.00 or 4.72 ppm (water) and the ^{13}C carrier was set at 126 ppm, with spectral widths of 39.8 ppm in $F_1(^{13}C)$ and 10.0 ppm in $F_2(^1H)$, 90 complex points in t_1, and 512 complex points in t_2. 2D ^1H–^{13}C CT-HSQC spectra optimized for nonaromatic resonances were acquired with the inept transfer delay set to 1.7 ms (slightly less than $^1/_4J_{CH}$) and the constant-time carbon evolution period set to 26 or 52 ms to refocus the carbon–carbon couplings of 38.5 Hz. A 180° carbonyl decoupling pulse was applied during carbon evolution. The spectra were acquired with the ^1H carrier set on water and the ^{13}C carrier set at 46 ppm, with spectral widths of 39.8 ppm in $F_1(^{13}C)$ and 10.0 ppm in $F_2(^1H)$, 128 complex points in t_1, and 512 complex points in t_2. 2D ^1H–^{13}C CT-HSQC–RELAY spectra were recorded using the same HSQC experiments with a 22-ms (aromatic resonances) or a 26-ms (nonaromatic resonances) ^1H WALTZ-17 mixing sequence inserted between the last refocusing period and data acquisition. In all heteronuclear experiments, GARP and WALTZ-16 modulation (Shaka et al., 1983) were used to decouple ^{13}C and ^{15}N, respectively, during acquisition.

3D ^{15}N-separated HOHAHA–HSQC (Marion et al., 1989a), NOESY–HMQC (Marion et al., 1989b; Kay et al., 1989), and HNHB (Archer et al., 1991) experiments were acquired on ^{15}N-labeled profilin in 93% H_2O/7% D_2O. 3D HOHAHA–HSQC spectra were acquired at 30 °C with 30- and 60-ms mixing times using a DIPSI-2 mixing sequence (Shaka et al., 1988). 3D NOESY–HMQC spectra were acquired at 37 °C with a 70-ms mixing time and at 30 °C with a 110-ms mixing time. The HOHAHA–HSQC, NOESY–HMQC, and HNHB experiments were acquired with spectral widths of 10.00, 22.9, and 11.76 ppm in $F_1(^1H)$, $F_2(^{15}N)$, and $F_3(^1H)$, respectively, and with 128 complex points in t_1, 32 complex points in t_2, 512 complex points in t_3, and 16 scans per t_3 point. A 3D $^{15}N/^{15}N$-separated NOESY–HMQC (Ikura et al., 1990; Frenkiel et al., 1990) spectrum was acquired with a 110-ms NOE mixing time. The spectrum was acquired with spectral widths of 32.2, 22.9, and 11.76 ppm in $F_1(^{15}N)$, $F_2(^{15}N)$, and $F_3(^1H)$, respectively, and with 64 complex points in t_1, 31 complex points in t_2, 512 complex points in t_3, and 32 scans per t_3 point. All 3D spectra were acquired with the ^1H carrier set on water and the ^{15}N carrier at 118.0 ppm.

The following 3D triple-resonance (1H, ^{13}C, ^{15}N) experiments were acquired on uniformly $^{15}N/^{13}C$-labeled profilin

Table I: ^{15}N, ^{13}C, and ^{1}H Resonance Assignments for Profilin at pH 6.45 and 30 °C[a]

residue	N	C^{α}	C^{β}	others
S1				
W2		59.9	29.7 (3.48, 3.19)	$C^{\delta 2}$ 128.0 (7.33), $C^{\epsilon 3}$ 120.3 (7.72), $C^{\zeta 2}$ 115.5 (7.12), $C^{\eta 3}$ 121.6 (6.71), C^{η} 124.4 (6.44), $N^{\epsilon 1}$ 129.3 (9.63)
Q3	118.3 (8.43)	58.5 (3.75)	28.5 (2.45, 1.97)	C^{γ} 33.1 (2.64, 2.45[b]), N^{ϵ} 115.3 (8.10, 6.97)
T4	114.0 (7.62)	66.2 (4.04)	68.6 (4.01)	C^{γ} 21.9 (1.13)
Y5	119.6 (7.37)	60.7 (4.88)	38.3 (3.32, 3.04)	C^{δ} 132.6 (7.12), C^{ϵ} 118.0 (6.44)
V6	115.9 (7.30)	66.7 (3.67)	32.3 (2.23)	C^{γ} 21.8 (0.94), 24.1 (0.97)
D7	118.3 (8.65)	57.9 (4.43)	40.9 (2.69, 2.68)	
T8	115.7 (9.05)	65.6 (4.26)	68.8 (4.26)	C^{γ} 21.8 (1.06)
N9	116.1 (7.59)	56.6 (4.43)	39.0 (3.20, 2.87)	N^{δ} 110.1 (7.70, 6.65)
L10	114.3 (6.94)	55.5 (4.67)	41.9 (2.40, 1.08)	C^{γ} 25.3 (1.56), C^{δ} 25.2 (0.83), 25.5 (0.80)
V11	122.3 (8.54)	66.4 (3.82)	31.6 (2.25)	C^{γ} 23.1 (0.88), 21.6 (0.96)
G12	105.3 (7.26)	47.1 (4.16, 4.03)		
T13	107.6 (7.11)	63.4 (4.31)	71.7 (4.30)	C^{γ} 21.8 (1.29)
G14	108.8 (8.17)	45.5 (4.28, 3.99)		
A15	122.0 (8.16)	52.9 (4.23)	20.8 (1.32)	
V16	103.0 (6.73)	59.2 (4.45)	34.8 (2.32)	C^{γ} 23.3 (0.74), 19.9 (0.54)
T17	114.8 (9.28)	63.3 (4.22)	69.0 (3.95)	C^{γ} 23.9 (1.13)
Q18	117.9 (7.34)	54.1 (4.23)	33.0 (0.83, 0.63)	C^{γ} 34.7 (2.18, 1.78), N^{ϵ} 111.3 (7.39, 6.83)
A19	120.8 (8.57)	51.5 (5.25)	25.8 (1.50)	
A20	117.2 (9.12)	51.8 (5.10)	23.4 (1.63)	
I21	117.3 (8.59)	61.3 (4.78)	41.1 (1.49)	C^{γ} 27.9 (1.17,[b] 1.13[b]), C^{δ} 14.9 (1.15), $C^{\gamma m}$ 16.9 (0.47)
L22	128.3 (9.32)	52.0 (4.74)	44.8 (1.36, 1.36)	C^{γ} 27.6 (1.40), C^{δ} 26.0 (0.64), 24.6 (0.58)
G23	102.9 (7.98)	44.4 (3.54, 3.53)		
L24	116.5 (7.59)	56.5 (3.87)	40.1 (1.59, 1.49)	C^{γ} 26.7 (1.35), C^{δ} 21.9 (0.50), 25.7 (0.85)
D25	114.0 (7.88)	52.8 (4.38)	40.3 (2.99, 2.62)	
G26	107.2 (8.07)	44.9 (4.05, 3.10)		
N27	117.2 (7.70)	53.4 (4.67)	39.4 (2.96, 2.75)	N^{δ} 113.8 (7.48, 6.89)
T28	118.4 (8.61)	65.4 (4.09)	70.4 (4.08)	C^{γ} 22.4 (1.15)
W29	129.8 (9.72)	56.2 (5.03)	29.8 (2.84, 2.75)	$C^{\delta 2}$ 123.1 (6.63), $C^{\epsilon 3}$ 119.7 (5.37), $C^{\zeta 2}$ 113.7 (7.40), $C^{\zeta 3}$ 121.2 (6.03), C^{η} 124.7 (6.98), $N^{\epsilon 1}$ 127.9 (10.49)
A30	119.5 (8.11)	52.3 (4.73)	22.8 (1.44)	
T31	114.9 (8.68)	60.6 (5.55)	71.7 (4.14)	C^{γ} 19.4 (1.40)
S32	125.8 (9.39)	58.9 (4.61)	64.4 (4.31, 3.90)	
A33	123.7 (8.57)	54.3 (4.23)	18.2 (1.44)	
G34	112.4 (8.89)	45.9 (4.21, 3.78)		
F35	122.8 (8.29)	55.9 (4.92)	40.3 (3.38, 2.74)	C^{δ} 131.8 (7.19), C^{ϵ} 130.9 (6.98), C^{ζ} 129.1 (6.65)
A36	132.5 (7.93)	51.0 (4.54)	19.8 (1.11)	
V37	125.0 (8.47)	61.9 (3.90)	32.2 (1.71)	C^{γ} 22.4 (0.34), 21.8 (0.89)
T38	121.3 (8.05)	60.9 (4.52)	67.7 (4.75)	C^{γ} 21.8 (1.24)
P39		65.9 (4.31)	31.4 (2.36, 1.92)	C^{γ} 28.4 (2.27, 2.13), C^{δ} 50.3 (3.91, 3.91)
A40	117.9 (8.07)	55.4 (4.13)	18.5 (1.40)	
Q41	119.2 (7.78)	58.4 (4.11)	28.1 (2.59, 2.00)	C^{γ} 34.4 (2.59, 2.59), N^{ϵ} 111.5 (7.53, 7.52)
G42	108.3 (8.95)	47.8 (4.10, 3.46)		
Q43	121.8 (8.81)	59.2 (3.88)	28.3 (2.17, 2.10)	C^{γ} 34.5 (2.50, 2.35), N^{ϵ} 110.1 (7.30, 6.71)
T44	118.6 (8.02)	67.3 (3.82)	68.6 (4.25)	C^{γ} 21.5 (1.18)
L45	122.0 (7.50)	57.9 (3.59)	42.2 (1.53, 1.49)	C^{γ} 26.7 (1.46), C^{δ} 25.2 (0.53), 23.3 (0.40)
A46	117.6 (8.37)	55.8 (4.05)	18.4 (1.35)	
S47	111.2 (8.08)	61.0 (4.26)	63.3 (4.00, 4.00)	
A48	125.2 (7.67)	53.4 (4.15)	18.9 (1.14)	
F49	113.4 (7.05)	62.3 (4.03)	39.0 (3.19, 2.59)	C^{δ} 132.0 (7.24), C^{ϵ} 131.5 (6.83), C^{ζ} 129.9 (6.99)
N50	114.2 (7.41)	54.1 (4.85)	39.8 (2.88, 2.87)	N^{δ} 112.9 (7.63, 6.87)
N51	115.9 (7.45)	53.6 (4.65)	38.6 (2.91, 2.69)	N^{δ} 110.1 (7.43, 6.98)
A52	127.5 (8.92)	52.8 (4.28)	18.8 (1.28)	
D53	119.7 (8.17)	59.9 (4.48)	37.5 (2.90, 2.63)	
P54		66.7 (4.40)	31.6 (2.36, 1.92)	C^{γ} 28.4 (2.07, 1.92), C^{δ} 50.6 (3.59, 3.49)
I55	109.8 (7.57)	62.9 (4.73)	38.7 (1.79)	C^{γ} 27.6 (1.27, 1.13[b]), C^{δ} 15.7 (0.41), $C^{\gamma m}$ 17.2 (0.80)
R56	128.5 (8.59)	61.0 (3.92)	30.0 (2.00, 1.95)	C^{γ} 29.5 (1.79, 1.54), C^{δ} 43.4 (3.25,[b] 3.19), N 84.5 (7.45)
A57	118.7 (7.72)	54.3 (4.42)	19.3 (1.52)	
S58	110.3 (8.06)	59.7 (4.62)	65.2 (3.97, 3.97)	
G59	111.2 (8.02)	45.7 (4.52, 4.08)		
F60	113.2 (8.12)	56.3 (4.90)	39.6 (2.94, 2.92)	C^{δ} 132.8 (6.75), C^{ϵ} 130.1 (6.71), C^{ζ} 127.7 (6.40)
D61	120.3 (8.72)	52.9 (5.77)	43.8 (2.61, 2.50)	
L62	118.5 (8.75)	55.2 (4.35)	46.3 (1.92, 1.44)	C^{γ} 27.0 (1.73), C^{δ} 28.5 (0.96), 25.3 (1.01)
A63	128.5 (9.55)	53.8 (4.13)	18.4 (1.36)	
G64	107.1 (8.14)	45.9 (4.01)		
V65	121.9 (7.60)	61.7 (3.93)	34.5 (1.79)	C^{γ} 21.6 (0.81), 21.7 (0.04)
H66	123.6 (8.04)	55.1 (4.82)	29.7 (2.96, 2.85)	$C^{\delta 2}$ 119.3 (6.92), $C^{\epsilon 1}$ 136.4 (8.57)
Y67	125.7 (8.59)	57.4 (4.10)	39.8 (2.02, 1.00)	C^{δ} 133.0 (6.29), C^{ϵ} 116.9 (6.36)
V68	116.3 (8.41)	61.2 (4.15)	33.3 (2.08)	C^{γ} 21.0 (1.04), 21.4 (1.00)
T69	123.7 (8.93)	64.4 (4.26)	68.0 (4.20)	C^{γ} 23.6 (1.00)
L70	130.0 (9.12)	55.5 (4.54)	44.5 (1.68, 1.54[b])	C^{γ} 27.2 (1.54[b]), C^{δ} 25.3 (1.01), 24.2 (0.96)
R71	117.9 (7.55)	55.2 (4.40)	33.2 (1.70, 1.29)	C^{γ} 26.3 (1.39, 1.11), C^{δ} 43.2 (2.55, 2.08), N 84.1 (7.00)
A72	126.5 (8.63)	52.6 (5.02)	20.9 (1.09)	
D73	124.2 (8.63)	53.5 (4.64)	41.5 (3.15, 2.79)	
D74	113.1 (8.33)	55.6 (4.89)	40.4 (2.82, 2.80)	
R75	120.5 (8.92)	57.2 (4.54)	33.0 (1.78, 1.78)	C^{γ} 28.6 (1.78[b]), C^{δ} 43.5 (3.26, 3.05), N 86.5 (7.25)

Table I (Continued)

residue	N	C^{α}	C^{β}	others
S76	114.2 (8.63)	58.3 (5.72)	65.2 (3.94, 3.36)	
I77	122.6 (8.75)	61.1 (4.67)	40.4 (1.18)	C^{γ} 28.2 (0.42), C^{δ} 13.5 (–0.57), $C^{\gamma m}$ 17.0 (0.19)
Y78	126.5 (9.06)	52.9 (5.93)	39.8 (3.35, 3.15)	C^{δ} 131.0 (7.11), C^{ϵ} 118.9 (6.83)
G79	109.1 (9.56)	44.2 (5.75, 3.33)		
K80	123.1 (9.49)	55.6 (5.20)	38.4 (1.93, 1.83)	C^{γ} 25.2 (1.79, 1.56), C^{δ} 30.0 (1.90[b]), C^{ϵ} 42.5 (3.15, 3.11)
K81	127.9 (8.52)	56.2 (4.49)	33.2 (1.48, 1.43)	C^{ϵ} 42.6 (3.05, 2.91)
G82	118.5 (9.12)	47.6 (4.09, 3.77)		
S83	123.1 (8.97)	58.9 (4.71)	63.5 (4.18, 3.99)	
A84	123.1 (8.07)	50.2 (4.46)	21.8 (1.59)	
G85	105.2 (6.95)	47.5 (3.99, 3.74)		
V86	114.8 (7.99)	58.9 (4.97)	34.3 (1.39)	C^{γ} 22.4 (0.54), 18.3 (0.04)
I87	129.4 (9.26)	58.4 (4.30)	38.6 (2.07)	C^{γ} 26.5 (1.49, 0.83), C^{δ} 9.7 (0.20), $C^{\gamma m}$ 17.6 (0.78)
T88	120.6 (8.28)	59.6 (6.13)	70.6 (4.02)	C^{γ} 23.7 (1.15)
V89	122.2 (8.66)	60.4 (5.19)	37.5 (1.58)	C^{γ} 23.3 (0.84), 22.9 (0.84)
K90	129.1 (8.99)	55.2 (4.56)	33.7 (1.09, 0.03)	C^{γ} 23.8 (1.52, 0.80), C^{δ} 29.7 (1.15[b]), C^{ϵ} 42.2 (2.83)
T91	118.2 (9.03)	60.6 (4.50)	66.0 (4.92)	C^{γ} 22.0 (1.06)
S92	115.3 (9.30)	62.6 (4.35)	62.6 (3.80, 3.80)	
K93	114.9 (8.22)	55.5 (4.54)	36.0 (2.32, 2.02)	C^{γ} 25.5 (1.43), C^{δ} 29.7 (1.85), C^{ϵ} 42.2 (3.06)
S94	116.2 (7.60)	57.2 (4.70)	69.0 (3.04, 3.04)	
I95	117.5 (8.72)	60.5 (4.41)	42.1 (1.22)	C^{γ} 27.6 (1.18, 0.51), C^{δ} 14.2 (0.71), $C^{\gamma m}$ 18.0 (0.71)
L96	126.0 (9.44)	54.1 (4.69)	44.2 (1.82, 1.19)	C^{γ} 27.6 (1.73), C^{δ} 24.7 (0.73), 26.2 (0.77)
V97	120.1 (8.84)	61.4 (4.60)	35.0 (2.15)	C^{γ} 22.3 (0.87), 20.6 (0.80)
G98	111.5 (9.37)	45.7 (4.97, 3.24)		
V99	127.7 (8.63)	61.9 (4.38)	34.0 (1.56)	C^{γ} 22.7 (0.63), 21.7 (0.87)
Y100	121.7 (8.47)	55.8 (5.17)	41.6 (3.16, 2.78)	C^{δ} 134.5 (7.11), C^{ϵ} 116.9 (6.58)
N101	119.9 (7.04)	50.7 (4.90)	39.9 (3.43, 2.82)	N^{δ} 109.8 (7.64, 6.76)
E102	112.8 (9.02)	58.4 (4.36)	28.9 (2.13, 2.11)	C^{γ} 36.2 (2.28, 2.28)
K103	117.8 (7.51)	56.3 (4.33)	32.7 (2.06, 1.86)	C^{γ} 25.5 (1.45, 1.43), C^{δ} 28.9 (1.69), C^{ϵ} 42.3 (3.02)
I104	122.6 (7.91)	59.9 (4.21)	42.0 (1.88)	C^{γ} 28.1 (1.52, 1.12), C^{δ} 14.4 (0.78), $C^{\gamma m}$ 17.2 (0.98)
Q105	124.6 (8.42)	53.9 (4.45)	27.9 (1.98, 2.17)	C^{γ} 33.9 (2.51), N^{ϵ} 113.0 (7.60, 6.90)
P106		65.5 (3.05)	32.0 (2.24,[b] 1.80)	C^{γ} 27.7 (2.15, 2.10), C^{δ} 50.4 (4.05, 3.71)
G107	102.1 (8.59)	46.7 (3.77, 3.76)		
T108	119.9 (7.46)	65.7 (3.98)	68.5 (4.31)	C^{γ} 22.0 (1.26)
A109	124.0 (6.80)	55.5 (3.92)	19.1 (1.08)	
A110	116.8 (8.20)	55.5 (3.79)	17.8 (1.35)	
N111	113.1 (7.57)	56.8 (4.34)	39.1 (2.91, 2.78)	N^{δ} 112.3 (7.63, 6.88)
V112	115.9 (7.32)	66.7 (3.79)	32.1 (2.06)	C^{γ} 23.2 (1.14), 21.6 (1.10)
V113	120.3 (7.68)	67.2 (3.45)	32.2 (1.92)	C^{γ} 23.2 (0.82), 22.7 (0.92)
E114	117.5 (8.79)	60.1 (3.96)	28.9 (2.04, 2.02)	C^{γ} 35.6 (2.38, 2.38)
K115	116.4 (7.97)	59.2 (4.20)	32.0 (2.02, 1.79)	C^{γ} 25.5 (1.65, 1.56), C^{δ} 28.9 (1.80,[b] 1.75), C^{ϵ} 42.4 (3.00)
L116	122.1 (7.59)	57.5 (4.42)	40.3 (1.94, 1.56[b])	C^{γ} 27.1 (1.56[b]), C^{δ} 23.0 (0.94), 27.1 (0.88)
A117	121.8 (8.36)	56.0 (3.81)	18.5 (1.39)	
D118	116.5 (8.11)	58.1 (4.42)	40.7 (2.87, 2.70)	
Y119	121.9 (7.91)	61.2 (4.29)	38.0 (3.33, 3.33)	C^{δ} 133.2 (7.06), C^{ϵ} 118.3 (6.88)
L120	120.7 (8.76)	58.5 (3.89)	41.6 (2.10, 1.51)	C^{γ} 27.5 (1.86), C^{δ} 22.1 (0.65), 26.5 (0.82)
I121	122.5 (9.38)	65.2 (4.25)	38.8 (1.89)	C^{γ} 31.0 (1.88, 1.07), C^{δ} 14.1 (0.91), $C^{\gamma m}$ 17.1 (0.94)
G122	108.1 (7.97)	46.8 (4.00, 3.99)		
Q123	116.7 (7.37)	54.9 (4.27)	30.4 (2.36, 2.00)	C^{γ} 33.6 (2.00, 2.00), N^{ϵ} 112.2 (6.94, 6.43)
G124	106.6 (7.87)	45.4 (4.02, 3.72)		
F125	125.0 (8.23)	58.8 (4.63)	41.8 (3.81, 2.78)	C^{δ} 131.5 (7.34), C^{ϵ} 131.5 (7.41), C^{ζ} 129.6 (7.31)

[a] In each column, ^{15}N and ^{13}C chemical shifts are listed first, and the corresponding ^{1}H chemical shifts are in parentheses. [b] Tentative assignment.

in 93% H_2O/7% D_2O: CBCA(CO)NH, CBCANH, C(CO)NH, H(CCO)NH, and $^{13}C/^{15}N$-separated NOESY–HMQC. The CBCA(CO)NH (Grzesiek & Bax, 1992a) and CBCANH (Grzesiek & Bax, 1992b) experiments were acquired with spectral widths of 67.2, 29.9, and 15.15 ppm in $F_1(^{13}C)$, $F_2(^{15}N)$, and $F_2(^{1}H)$, respectively, and with 52 complex points in t_1, 32 complex points in t_2, 512 complex points in t_3, and 16 scans per t_3 point for the CBCA(CO)NH and 32 scans per t_3 point for the CBCANH. The C(CO)NH (Grzesiek et al., 1993) spectrum was acquired with spectral widths of 73.6, 29.9, and 15.15 ppm in $F_1(^{13}C)$, $F_2(^{15}N)$, and $F_3(^{1}H)$, respectively, and with 57 complex points in t_1, 30 complex points in t_2, 512 complex points in t_3, and 32 scans per t_3 point. The H(CCO)NH (Grzesiek et al., 1993) spectrum was acquired with spectral widths of 13.33, 29.9, and 18.51 ppm in $F_1(^{1}H)$, $F_2(^{15}N)$, and $F_3(1H)$, respectively, and with 68 complex points in t_1, 32 complex points in t_2, 512 complex points in t_3, and 32 scans per t_3 point. Both the C(CO)NH and the H(CCO)NH experiments were acquired with a 16-ms mixing time using a ^{13}C DIPSI-2 mixing sequence (Shaka et al., 1988). In all of the triple-resonance experiments, the carrier was set at 46 ppm for $C^{\alpha/\beta}$ pulses and at 56 ppm for C^{α} pulses, and the pulse lengths were adjusted so that they did not excite the ^{13}CO nuclei. The ^{1}H carrier was set on water, and the ^{15}N carrier was set at 118.0 ppm.

A 3D $^{13}C/^{15}N$-separated NOESY–HMQC experiment was acquired with ^{13}C evolution in t_1 (F_1) on uniformly $^{15}N/^{13}C$-labeled profilin in 93% H_2O/7% D_2O. In this 3D NOESY experiment, the initial inept transfer of magnetization from ^{1}H to ^{15}N was replaced by an inept transfer from ^{1}H to ^{13}C. The data were acquired with spectral widths of 67.2, 22.9, and 11.76 ppm in $F_1(^{13}C)$, $F_2(^{15}N)$, and $F_3(^{1}H)$, respectively, and with 64 complex points in t_1, 32 complex points in t_2, 512 complex points in t_3, and 32 scans per t_3 point. The ^{13}C, ^{15}N, and ^{1}H carrier frequencies were 46.0, 118.0, and 4.72 ppm, respectively.

The 4D $^{13}C/^{13}C$-separated HMQC–NOESY–HMQC experiment using pulsed field gradients was acquired at 600 MHz as described by Vuister et al. (1993). The spectrum was recorded as a 4D matrix of 16 × 64 × 17 × 384 complex points in $F_1(^{13}C) \times F_2(^{1}H) \times F_3(^{13}C) \times F_4(^{1}H)$, with spectral widths of 20.7, 8.96, 20.7, and 11.90 ppm in $F_1(^{13}C)$, $F_2(^{1}H)$,

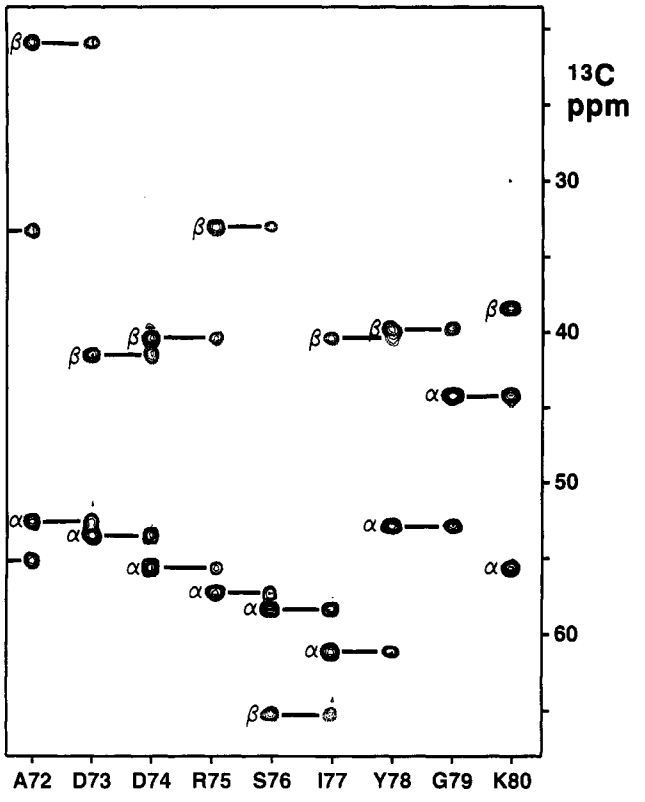

FIGURE 2: Sequential strips extracted from the CBCANH experiment. Intraresidue correlations are labeled with Greek symbols. We note that all interresidue correlations were also observed in the CBCA(CO)NH spectrum.

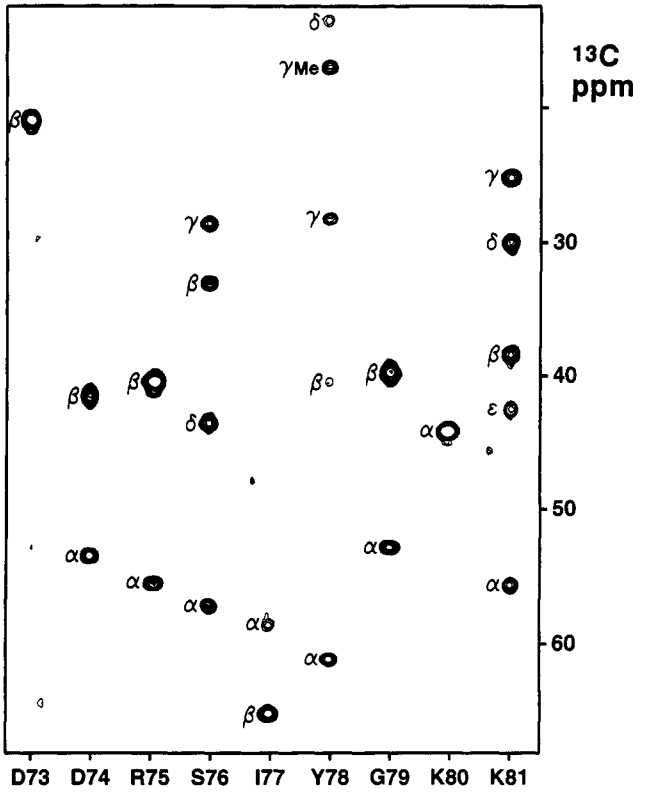

FIGURE 3: Strips extracted from the C(CO)NH experiment. Correlations from the amide to the side-chain carbon resonances of the preceding residue are indicated by Greek symbols.

$F_3(^{13}C)$, and $F_4(^1H)$, respectively. The ^{13}C carrier was set at 63.7 ppm, and the ^1H carrier was set at 4.72 ppm for a mild water presaturation pulse and then at 4.05 ppm for the remainder of the pulse sequence. The pulse field gradients had a strength of 7 G/cm.

RESULTS

A ^1H–^{15}N HSQC spectrum for uniformly ^{15}N-labeled profilin is shown in Figure 1. The excellent signal to noise ratio is comparable to that observed in HSQC spectra of uniformly enriched staphylococcal nuclease (Baldisseri et al., 1991) and *Escherichia coli* protein III^{glc} (Pelton et al., 1991), indicating that the sample is highly and uniformly ^{15}N-enriched.

The CBCA(CO)NH and CBCANH triple-resonance experiments, which rely solely on one- and two-bond scalar couplings, were used to sequentially assign the protein backbone. In the CBCANH experiment, H^β magnetization is transferred to C^β and then from C^β to C^α. The C^α magnetization is then transferred to both the intraresidue ^{15}N and the ^{15}N of the succeeding residue via the $^1J_{C\alpha N}$ and $^2J_{C\alpha N}$ couplings, respectively (Grzesiek & Bax, 1992b), and then finally to the amide protons for detection. Thus, amide proton and nitrogen signals of each amino acid were correlated with both the intraresidue α and β carbons and the α and β carbons of the preceding residue (Figure 2). In the complementary CBCA(CO)NH experiment, the C^α magnetization is transferred to the intraresidue carbonyl carbon and then to the amide nitrogen of the succeeding residue via the large $^1J_{C\alpha C'}$ and $^1J_{C'N}$ couplings. Here, in contrast with the CBCANH experiment, each backbone amide is correlated with the α and β carbons of the preceding residue only (Grzesiek & Bax, 1992a). Using the information from the CBCA(CO)NH experiment, it was simple to distinguish intraresidue from interresidue correlations in the CBCANH (Figure 2). Additionally, in the CBCANH, the C^α resonance of Gly and the C^β resonances of all other residues are opposite in sign to the C^α resonances (Grzesiek & Bax, 1992b), which made it easy to distinguish C^β from C^α resonances (Figure 2).

Stretches of amide resonances were aligned sequentially by matching the intraresidue C^α and C^β chemical shifts with the interresidue C^α and C^β chemical shifts of its neighbor. By subsequently matching pairs and longer segments, we were able to align all of the non-proline resonances in sequential stretches ranging from 3 to 17 residues long.

The C^α and C^β chemical shifts were then used to calculate the probability of each C^α/C^β pair belonging to a particular amino acid type (Grzesiek & Bax, 1993). Gly residues were easily identified by their distinct upfield chemical shift, as well as by the presence of only one negative intraresidue cross peak. Thr, Ser, and Ala residues were readily identified by their unique pairs of C^α/C^β chemical shifts. Once the amino acid type for the Thr, Ser, Ala, and Gly residues was known, it was straightforward to assign each stretch of amino acids to a unique section of the protein sequence. These assignments were confirmed by checking the amino acid type probabilities (Grzesiek & Bax, 1993) for the other residues in each stretch. These assigned stretches were then aligned in sequential order, and the alignment was confirmed by matching the interresidue C^α and C^β signals of the first residue in a sequence with the intraresidue C^α and C^β signals of the last residue in the preceding sequence. Continuous stretches of amino acids were determined from Q3–T38, A40–D53, I55–Q105, and G107–F125. Except for the first two residues, breaks in the sequential alignment occurred only at proline residues. We note that the backbone assignments were completed in less than 8 h after the CBCA(CO)NH and CBCANH data were processed.

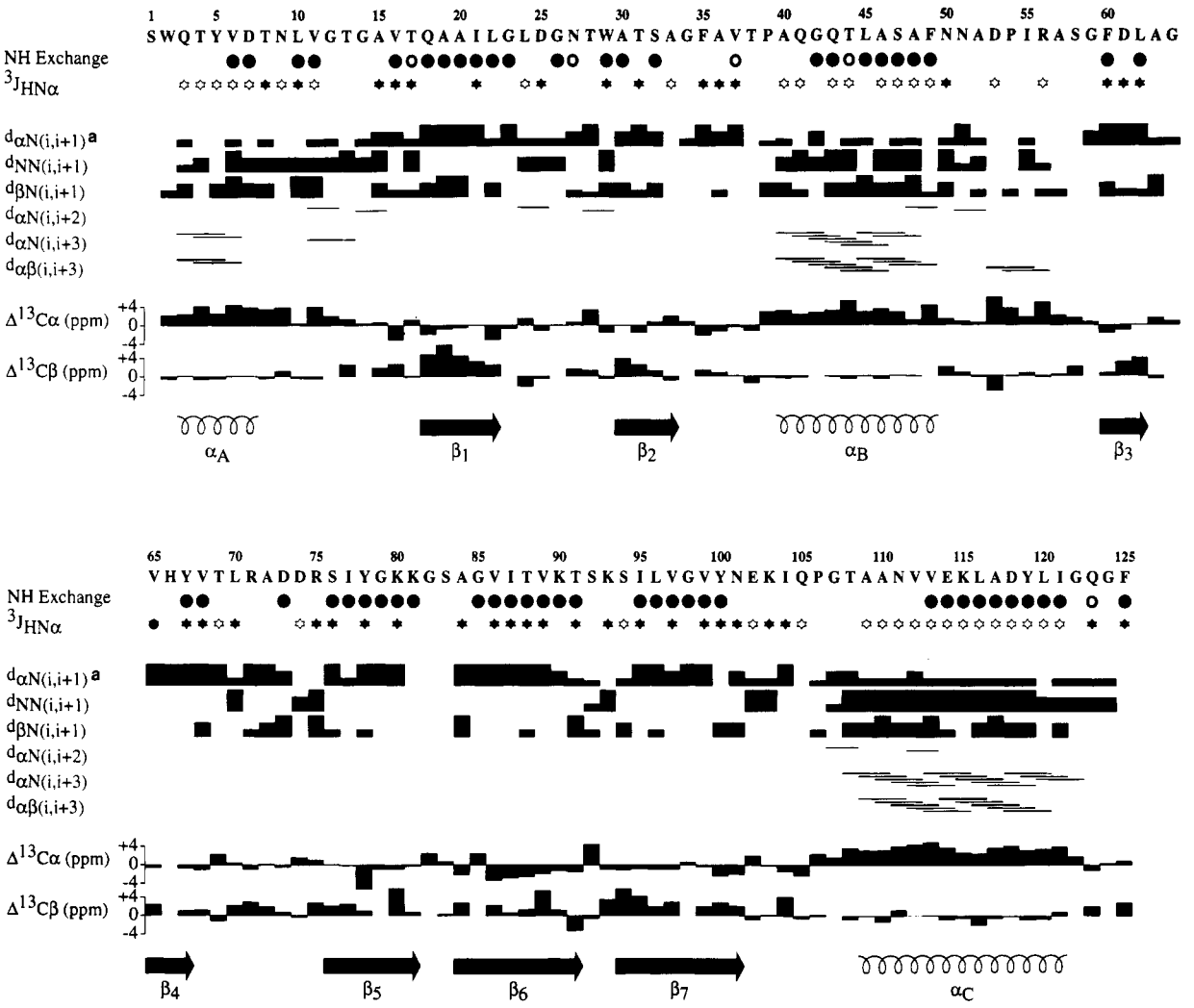

FIGURE 4: Diagram of short-range NOE connectivities, hydrogen exchange rates, and coupling constant data for profilin. The NOE correlations were determined from 3D and 4D NOESY spectra at 30 and 37 °C. The height of the bar indicates the strength of the NOE correlation (strong, medium, or weak). Open and filled circles indicate residues with amide H^N resonances that are not fully exchanged 8 min and 1 h, respectively, after the protein is dissolved in D_2O at 30 °C and pH 6.45. Open and filled stars indicate small (<6 Hz) and large (>8 Hz) $^3J_{HNH\alpha}$ coupling constants, respectively. (a) Only the strongest of the two possible glycine H^α–H^N_{i+1} NOEs is shown.

Correlations observed in 3D ^{15}N-separated HOHAHA–HSQC experiments acquired with 30- and 60-ms mixing times (a) further confirmed the amino acid type assignments and (b) provided initial ^1H side-chain assignments. H^α resonances and many H^β resonances were readily identified in the short mixing time HOHAHA–HSQC experiment, while H^γ and additional H^β resonances were identified in the longer mixing time experiment. H^β resonance assignments were confirmed by the observation of cross peaks in the HNHB experiment. These results and information derived from 3D H(CCO)NH, 2D ^1H–^{13}C CT-HSQC, and CT-HSQC–RELAY experiments provided essentially complete side-chain assignments, as described below.

The aromatic side-chain protons were initially identified from cross-peak patterns in the 2D ^1H HOHAHA experiment following standard methodology (Wüthrich, 1986). These assignments were confirmed and extended to aromatic carbon resonances from the cross-peak patterns in the 2D ^1H–^{13}C CT-HSQC and CT-HSQC–RELAY experiments acquired with parameters optimized for aromatic side-chain resonances. The aromatic side-chain type assignments were correlated with backbone sequential assignments through the $^1H^\delta$ and $^{13}C^\delta$ signals identified in the 3D ^{15}N-separated NOESY–HMQC and $^{13}C/^{15}N$-separated NOESY–HMQC experiments, respectively.

The C(CO)NH and H(CCO)NH experiments were used to correlate aliphatic side-chain carbon and aliphatic side-chain proton signals, respectively, to the amide resonance of the succeeding residue (Grzesiek et al., 1993). In this way, each sequentially assigned amide was correlated with both the aliphatic side-chain carbons and protons of the preceding residue. The CBCA(CO)NH experiment was used to identify C^α and C^β carbon signals in the C(CO)NH spectrum, and the remaining aliphatic side-chain resonances in the C(CO)NH were relatively straightforward to assign from the carbon chemical shift (Figure 3). In a similar fashion, the 3D HOHAHA–HSQC was used to identify H^α, H^β, and other aliphatic side-chain protons in the H(CCO)NH spectrum, and the remaining side-chain protons in the H(CCO)NH experiment were tentatively assigned to particular side-chain protons. The 2D ^1H–^{13}C CT-HSQC and CT-HSQC–RELAY experiments were used to confirm and complete aliphatic side-chain proton and carbon assignments.

The ^1H, ^{13}C, and ^{15}N resonance assignments are summarized in Table I. Complete backbone resonance assignments (H^N, N, C^α, H^α) were determined for all residues except S1, the amide H^N/N and H^α of W2, and the amide N of proline residues. Side-chain ^1H, ^{13}C, and ^{15}N resonance assignments were determined for 97% of all side-chain atoms. The availability of this comprehensive information regarding chemical shifts immediately opens the way to determine the profilin residues that interact with PIP, PIP_2, poly(proline), and actin through measurements of protection against hydrogen exchange and chemical shift perturbations.

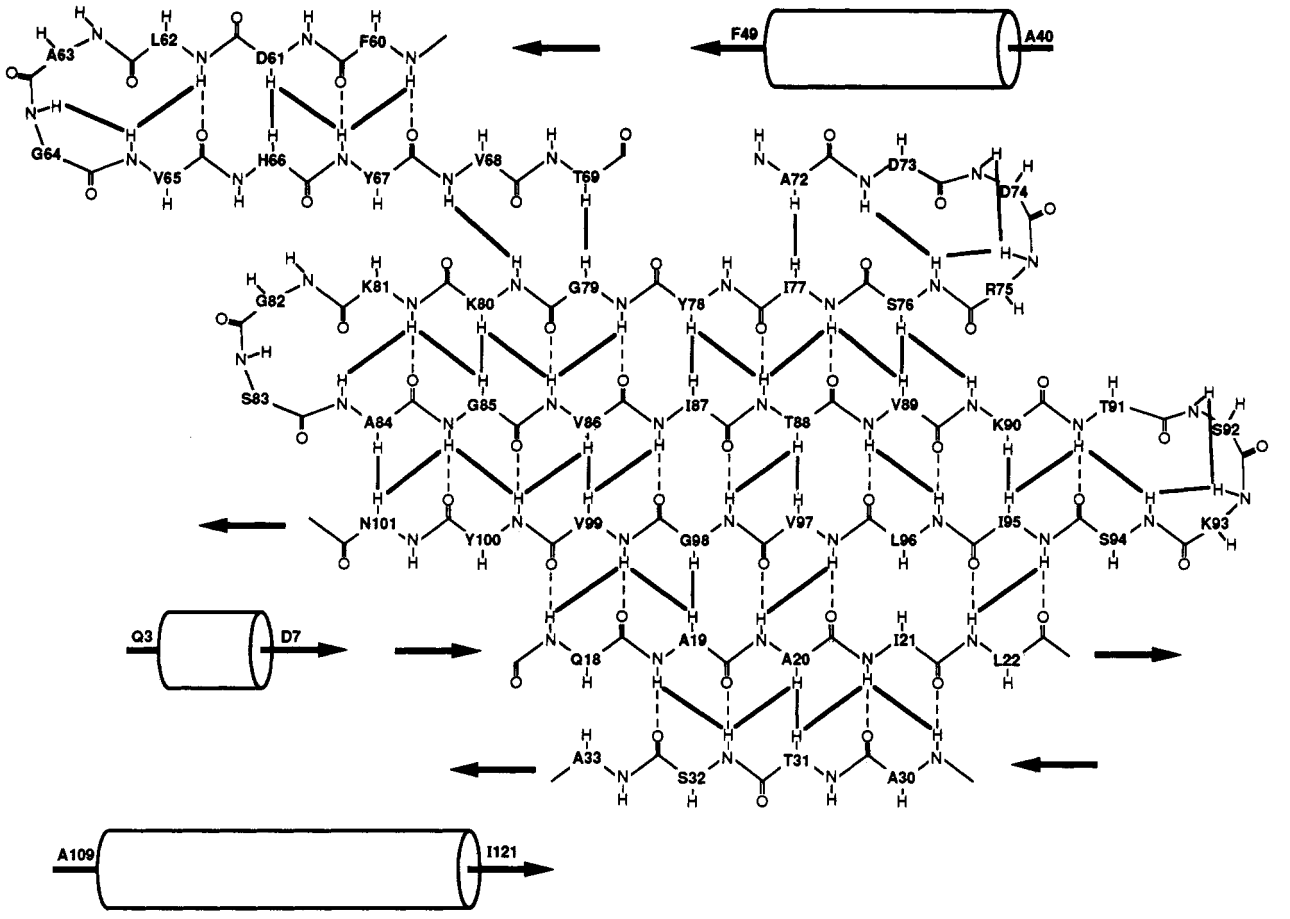

FIGURE 5: Schematic diagram of the secondary structure and β-sheet topology of profilin showing the long-range H^N_i–H^N_j and H^α_i–H^α_j NOE correlations (solid lines) observed in NOESY spectra. Dashed lines represent hydrogen bonds derived from hydrogen exchange rates and NOE patterns.

Once the sequential assignments were complete, NOE correlations from 3D NOESY–HMQC, 3D $^{13}C/^{15}N$-separated NOESY–HMQC, 3D $^{15}N/^{15}N$-separated NOESY–HMQC, and 4D $^{13}C/^{13}C$-separated HMQC–NOESY–HMQC experiments were used to determine interproton distance constraints. NOE correlations from the 70-ms 3D NOESY–HMQC and the 110-ms 4D $^{13}C/^{13}C$-separated HMQC–NOESY–HMQC experiments were categorized as strong, medium, and weak. The HSQC hydrogen exchange experiment was used to determine which protons were in slow exchange and, therefore, most likely involved in interresidue hydrogen bonds. Dihedral constraints for backbone ϕ angles were determined from $^3J_{HNH\alpha}$ coupling constants calculated from splittings in the HMQC-J experiment and H^α/H^N intensity ratios in the 30-ms 3D HOHAHA–HSQC experiment. Only coupling constants greater than 8 Hz or less than 6 Hz were used for dihedral constraints. Short-range NOEs, hydrogen exchange data, and coupling constant data are summarized in Figure 4.

The secondary structure and β-sheet topology of profilin in solution (Figure 5) were derived from the information summarized in Figure 4 together with cross-strand NOEs. The central feature of the profilin structure is a five-stranded antiparallel β-sheet made up of β-strands S76–K81, A84–T91, S94–N101, Q18–L22, and A30–A33. There are two antiparallel β-strands, F60–L62 and V65–V67, joined by a tight turn. Residues within the β-strands were in an extended conformation, as indicated by strong H^α_i–H^N_{i+1} NOE correlations and large $^3J_{HNH\alpha}$ (>8 Hz) coupling constants (Figure 4). Long-range H^N_i–H^N_j, H^α_i–H^N_j, and H^α_i–H^α_j NOE correlations were used to determine the alignment of the β-strands in a sheet structure (Figure 5). Amide protons with slow exchange rates correlated well with the hydrogen-bonding pattern expected for the antiparallel β-sheets.

Profilin has three α-helices: a short N-terminal helix from Q3 to D7, a central helix from A40 to F49, and a long C-terminal helix from A109 to I121. All three helical domains exhibit predominantly the classical NMR features of well-defined α-helices: medium H^N_i–H^N_{i+1}, weak H^α_i–H^N_{i+1}, medium H^α_i–H^β_{i+3}, and weak H^α_i–H^N_{i+3} NOE correlations, as well as slow amide hydrogen exchange rates and small $^3J_{HNH\alpha}$ (<6 Hz) coupling constants (Figure 4). In addition, the α-carbon chemical shifts are shifted downfield as expected for helical domains (Spera & Bax, 1991). There are additional helix-like tight turns at the ends of the first and second helices, as indicated by medium H^N_i–H^N_{i+1}, weak H^α_i–H^N_{i+1}, and downfield-shifted C^α resonances. Profilin contains three proline residues. All X–Pro bonds are trans, based upon the observation of strong X(H^α)–Pro(H^δ) NOEs for P39 and P106 and medium X(H^β)–Pro(H^δ) and X(H^N)–Pro(H^δ) NOEs for P54.

DISCUSSION

Examination of Figure 5 shows that a large percentage of the profilin sequence is composed of regular secondary structure elements (helix and sheet) and tight turns. It seems likely that, as a consequence of its well-defined structure, profilin behaves as a compact globule in solution. Such behavior would maximize T_2 values and account for the uniformly high-quality spectra that were obtained for profilin. The spectra, in turn, made possible the rapid assignment of the profilin signals.

It is noteworthy that residues found in helical regions show a large degree of homology when sequences of various members

of the profilin family are compared using the alignment reported by Pollard and Rimm (1991). Of particular interest is the long C-terminal helix. Residues 95–125 have been postulated to represent an ancient actin-binding site from chemical cross-linking of K115 of profilin with E364 of actin (Vandekerckhove et al., 1989) and C-terminal sequence homology between profilin and other actin-binding proteins (Ampe & Vandekerckhove, 1987; Andre et al., 1988). This suggests that the well-defined C-terminal helix may be a common structural element in several families of actin-binding proteins.

The determination of the secondary structure of the profilin molecule helps to clarify a long-standing uncertainty regarding the alignment of profilin sequences from various species, as discussed in Pollard and Rimm (1991). Given the five-stranded antiparallel β-sheet, the alignment of Takagi et al. (1990) illustrated in Pollard and Rimm (1991) seems less likely than alternative alignments. The Takagi alignment gives a superior match of residues between vertebrate and invertebrate profilins, but according to this model the vertebrate profilin would have an additional four residues inserted between residues 79 and 80 and five residues between residues 85 and 86 relative to *Acanthamoeba* profilin—both disrupting the β-sheet. This suggests that, if the Takagi alignment is correct, the secondary structure of vertebrate profilin differs from that of *Acanthamoeba* profilin. This ambiguity will be resolved when other structures become available.

Further elucidation of the profilin structure–function relationship must await the determination of the three-dimensional structure of the protein. Fortunately, because of the extensive regular secondary structure of profilin and the high-quality NOESY data obtained for the protein, the 3D structure is rapidly emerging, and a low-resolution structure should be available imminently.

ACKNOWLEDGMENT

We gratefully acknowledge Dr. E. E. Lattman for initiating the collaboration that made this work possible and for helpful discussions. We acknowledge Drs. D. Garrett, S. Grzesiek, R. Powers, G. Vuister, and F. Delaglio for generously providing computer software. We also thank G. Vuister for acquisition and processing of the 4D NOESY spectrum. We thank R. Tschudin for expert technical support and Dr. A. Bax for helpful discussions and preprints of the triple-resonance experiments.

SUPPLEMENTARY MATERIAL AVAILABLE

Table listing the $^3J_{HNH\alpha}$ couplings (Table S1) (1 page). Ordering information is given on any current masthead page.

REFERENCES

Ampe, C., & Vandekerckhove, J. (1987) *EMBO J. 6*, 4149–4157.

Andre, E., Lottspeich, F., Schleicher, M., & Noegel, A. (1988) *J. Biol. Chem. 263*, 722–727.

Archer, S. J., Ikura, M., Torchia, D. A., & Bax, A. (1991) *J. Magn. Reson. 95*, 636–641.

Baldisseri, D. M., Torchia, D. A., Poole, L. B., & Gerlt, J. A. (1991) *Biochemistry 30*, 3628–3633.

Bax, A., & Davis, G. (1985) *J. Magn. Reson. 65*, 355–360.

Bax, A., & Grzesiek, S. (1993) *Acc. Chem. Res. 26*, 131–138.

Bodenhausen, G., & Ruben, D. J. (1980) *Chem. Phys. Lett. 69*, 185–189.

Braunschweiler, L., & Ernst, R. R. (1983) *J. Magn. Reson. 53*, 521–528.

Carlsson, L., Nystrom, L. E., Sundkvist, I., Markey, F., & Lindberg, U. (1977) *J. Mol. Biol. 115*, 465–483.

Clore, G. M., & Gronenborn, A. M. (1989) *Crit. Rev. Biochem. Mol. Biol. 24*, 479–564.

Frenkiel, T., Bauer, C., Carr, M. D., Birdsall, B., & Feeney, J. (1990) *J. Magn. Reson. 90*, 420–425.

Garrett, D. S., Powers, R., Gronenborn, A. M., & Clore, G. M. (1991) *J. Magn. Reson. 95*, 214–220.

Goldschmidt-Clermont, P. J., Machesky, L. M., Baldassare, J. J., & Pollard, T. D. (1990) *Science 247*, 1575–1578.

Goldschmidt-Clermont, P. J., Kim, J., Machesky, L. M., Rhee, S., & Pollard, T. D. (1991) *Science 251*, 1231–1233.

Grzesiek, S., & Bax, A. (1992a) *J. Am. Chem. Soc. 114*, 6291–6293.

Grzesiek, S., & Bax, A. (1992b) *J. Magn. Reson. 99*, 201–207.

Grzesiek, S., & Bax, A. (1993) *J. Biomol. NMR 3*, 185–204.

Grzesiek, S., Döbeli, H., Gentz, R., Garotta, G., Labhardt, A. M., & Bax, A. (1992) *Biochemistry 31*, 8180–8190.

Grzesiek, S., Anglister, J., & Bax, A. (1993) *J. Magn. Reson. B101*, 114–119.

Hartwig, J. H., Changers, K. A., Hopica, K. L., & Kwiatkowski, D. J. (1989) *J. Cell Biol. 109*, 1571–1579.

Ikura, M., Bax, A., Clore, G. M., & Gronenborn, A. M. (1990) *J. Am. Chem. Soc. 112*, 9020–9022.

Kaiser, D. A., Goldschmidt-Clermont, P. J., Levine, B., & Pollard, T. D. (1989) *Cell Motil. Cytoskel. 14*, 251–262.

Kay, L. E., & Bax, A. (1990) *J. Magn. Reson. 86*, 110–126.

Kay, L. E., Marion, D., & Bax, A. (1989) *J. Magn. Reson. 84*, 72–84.

Machesky, L. M., Goldschmidt-Clermont, P. J., & Pollard, T. D. (1990) *Cell Regul. 1*, 937–950.

Marion, D., Driscoll, P. C., Kay, L. E., Wingfield, P. T., Bax, A., Gronenborn, A. M., & Clore, G. M. (1989a) *Biochemistry 28*, 6150–6156.

Marion, D., Kay, L. E., Sparks, S. W., Torchia, D. A., & Bax, A. (1989b) *J. Am. Chem. Soc. 111*, 1515–1517.

Messerle, B. A., Wider, G., Otting, G., Weber, C., & Wüthrich, K. (1989) *J. Magn. Reson. 85*, 608–613.

Pelton, J. G., Torchia, D. A., Meadow, N. D., Wong, C.-Y., & Roseman, S. (1991) *Biochemistry 30*, 10043–10057.

Pollard, T. D., & Rimm, D. L. (1991) *Cell Motil. Cytoskel. 20*, 169–177.

Shaka, A. J., Keeler, J., & Freeman, R. (1983) *J. Magn. Reson. 53*, 313–340.

Shaka, A. J., Lee, C. J., & Pines, A. (1988) *J. Magn. Reson. 77*, 274–293.

Spera, S., & Bax, A. (1991) *J. Am. Chem. Soc. 113*, 5490–5492.

Takagi, T., Mabuchi, I., Hosoya, H., Furuhashi, K., & Hatano, S. (1990) *Eur. J. Biochem. 192*, 777–781.

Vandekerckhove, J. S., Kaiser, D. A., & Pollard, T. D. (1989) *J. Cell Biol. 109*, 619–626.

Vuister, G. W., & Bax, A. (1992) *J. Magn. Reson. 98*, 428–435.

Vuister, G. W., Clore, G. M., Gronenborn, A. M., Powers, R., Garrett, D. S., Tschudin, R., & Bax, A. (1993) *J. Magn. Reson. B101*, 210–213.

Wüthrich, K. (1986) *NMR of Proteins and Nucleic Acids*, John Wiley, New York.